Superalloys 2004
Edited by K.A. Green, T.M. Pollock, H. Harada, T.E. Howson, R.C. Reed, J.J. Schirra, and S. Walston
TMS (The Minerals, Metals & Materials Society), 2004

ISSUES IN PROCESSING BY THE LIQUID-Sn ASSISTED DIRECTIONAL SOLIDIFICATION TECHNIQUE

A.J. Elliott[1], G.B. Karney[2], M.F.X. Gigliotti[3], T.M. Pollock[1]
[1]University of Michigan; Materials Science and Engineering; 2300 Hayward Street; Ann Arbor, MI 48109-2136, USA
[2]Oxford University; Materials Science; Parks Road; Oxford, OX1 3PH, UK
[3]General Electric Global Research; One Research Circle; Niskayuna, NY 21309, USA

Keywords: LMC, dendrite, solidification, columnar grain

Abstract

Aspects of the liquid-tin assisted directional solidification process that have the greatest impact on cooling conditions at the solidification front have been investigated. Thermal conditions within the mushy zone of the casting and outside the mold in the tin bath were characterized experimentally as a function of casting parameters. Macroscopic casting defects were identified and microstructural analysis was performed, including measurement of primary and secondary dendrite arm spacings (PDAS and SDAS). Process parameters that most strongly influenced casting quality included withdrawal rate, superheat, and degree of insulation on top of the coolant bath. Control of the position of the solidification front relative to the coolant bath was essential for production of defect free castings.

Introduction

The need for high efficiency, high operating temperature industrial gas turbines (IGTs) has motivated the introduction of directionally solidified (DS) and single crystal (SX) nickel-base superalloy castings into power generation turbines. Unfortunately, SX and DS casting techniques, which have been optimized for aero-engine scale blades, are not easily scaled up for solidification of the physically massive castings required for large IGTs. The industrially prevalent Bridgman "high rate solidification" process[1, 2] relies primarily on radiation cooling except for the first few centimeters of the casting above the copper chill plate.[3-5] Casting IGT components using this technique results in relatively low thermal gradients for the required section sizes and requires very slow withdrawal rates to maintain columnar dendrite orientation. This results in high defect occurrence and high casting rejection rates.[5-7] Freckle-type defects, small chains of equiaxed grains that form due to convective instabilities in the mushy zone of the solidifying casting, are a common defect in DS castings. Freckle formation is influenced by the primary dendrite arm spacing (PDAS), thermal gradient, withdrawal rate, and, consequently, cooling rate during solidification.[8, 9] Therefore, higher thermal gradients and faster withdrawal rates are essential to reducing grain defects in DS IGT castings. This has motivated a number of investigations on new high gradient solidification processes.[4-6, 10-16]

Liquid metal cooling (LMC) is a process which was originally developed in the 1970s to achieve the high gradient conditions required to cast DS eutectic alloys.[17, 18] During the LMC process, cooling is achieved by direct withdrawal of the molten superalloy, contained in an investment mold, from a heater into a container of low melting temperature metal coolant. LMC with an aluminum coolant has been utilized for production of aero-engine blades in the former Soviet Union.[19, 20] More recent investigations using tin and aluminum as cooling media indicate benefits of the LMC process for IGT components, including thermal gradients at least double those achieved with the conventional process, increased withdrawal rates and reduced process time.[4-6, 13-16, 21] Tin, however, may be more advantageous than aluminum because of its significantly lower melting temperature (232 °C vs. 660 °C).[14] Additionally, although tin is quite dense compared to other possible coolants, this permits a baffle of small alumina beads to float on the surface of the liquid tin, serving as a conforming thermal barrier between the heating and cooling zones of the furnace.[22]

While LMC processes have been reported to be beneficial, there have not been detailed comparisons between conventional and LMC casting processes in terms of cooling rate, microstructure, defect reduction and heat flow analysis. We have recently assessed the benefits of the LMC-Sn process over the conventional Bridgman technique in DS solidification experiments on castings with large cross-sectional areas.[15, 16] The LMC-Sn process produced very high thermal gradients and reduced casting defects under conditions where the solid-liquid interface was located near or just below the surface of the cooling bath. The current work focuses on identification of the features of the LMC process that are central to improving solidification. Additional experiments have been conducted to isolate the process parameters that most strongly influence dendritic growth and defect formation. Selected results from prior experiments[15, 16] are included for comparison.

Experimental Procedures

A unique furnace designed for operation in both Bridgman and LMC modes with identical investment molds was utilized to make large (5 kg) columnar grained nickel-base superalloy castings, Figure 1. The liquid metal coolant bath contained approximately 500 kg of Sn. The approximately 10 mm thick floating baffle on the coolant bath consisted of small alumina beads ranging in diameter from 0.6 to 2.5 mm. Full details of the casting unit, data acquisition system, and casting dimensions have been previously reported.[16]

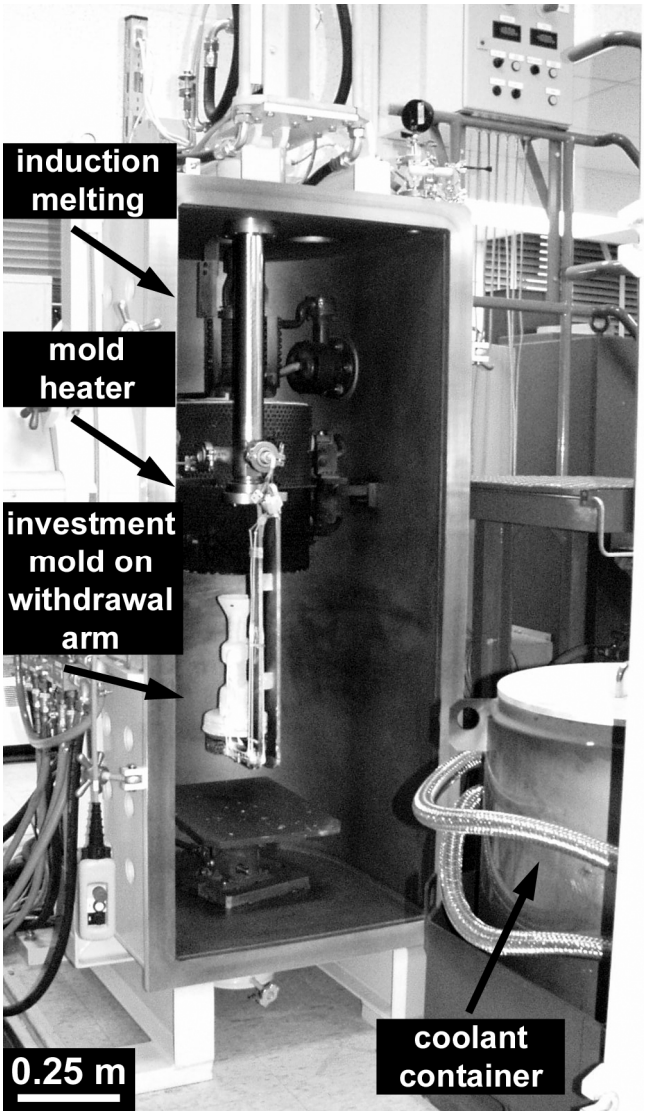

(a)

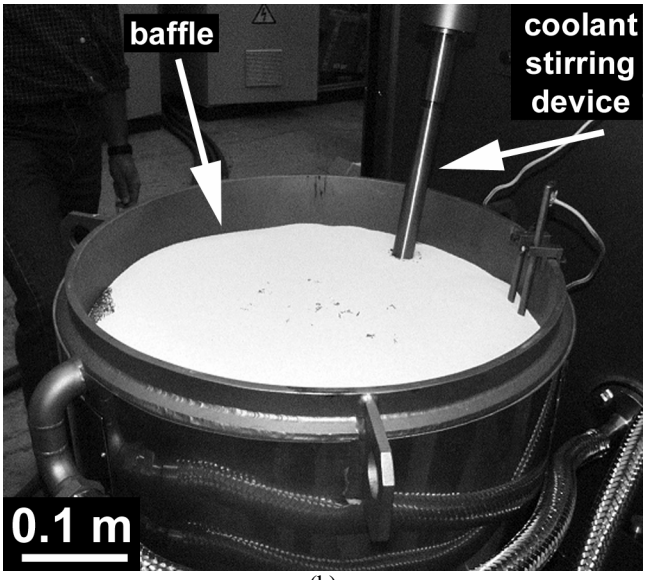

(b)

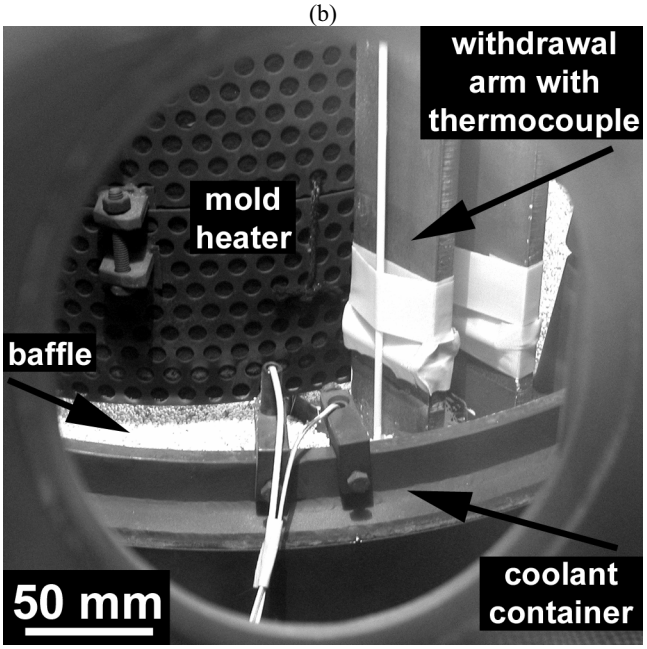

(c)

Figure 1. The experimental Bridgman/LMC directional solidification furnace (a). The coolant container filled with tin covered by the baffle of alumina beads (b). The coolant container positioned below the mold heater during solidification (c).

The castings for experiments reported here were designed to be representative of large IGT components, Figure 2. The castings had three stepped cross-sections having a constant width of 95 mm and thicknesses of 10 mm, 38 mm, and 51 mm. All castings were fabricated using ingots from a single heat of a columnar grain variant of the first generation single crystal alloy René N4.[23, 24] The nominal composition of the material was Ni -9.7Cr -8.0Co -6.0W -4.7Ta -4.2Al -3.5Ti -0.4Nb -0.15Hf -0.07C -0.008B (wt. %). In the previous set of experiments,[16] Bridgman and LMC castings were made using identical process parameters at a withdrawal rate of 2.5 mm/min for a direct comparison of the two processes. Additional LMC castings were made using the same casting conditions, but at withdrawal rates up to 8.5 mm/min, to assess the capability for increased withdrawal rates. Additional experiments reported here were conducted to investigate individual LMC process parameters and to isolate their influence on solidification using the best conditions from the first round of experiments as a baseline. The previous set of experiments demonstrated that a casting withdrawn at 6.8 mm/min experienced very high thermal gradients and was free of defects outside the starter region. Therefore the 6.8 mm/min withdrawal rate and all other casting parameters associated with this prior experiment were used as a "baseline" condition. Castings with "baseline" conditions except for either increased superheat (+50°C) or without the floating baffle of alumina beads, referred to as the "high superheat" and "no baffle" experiments respectively, were conducted. All castings were instrumented with several thermocouples inserted through the mold wall into the casting to directly determine cooling rates, and to locate the position of the solid-liquid (S-L) interface. Coolant bath temperatures were recorded using thermocouples positioned in the Sn bath approximately 10 mm from the inner wall of the container

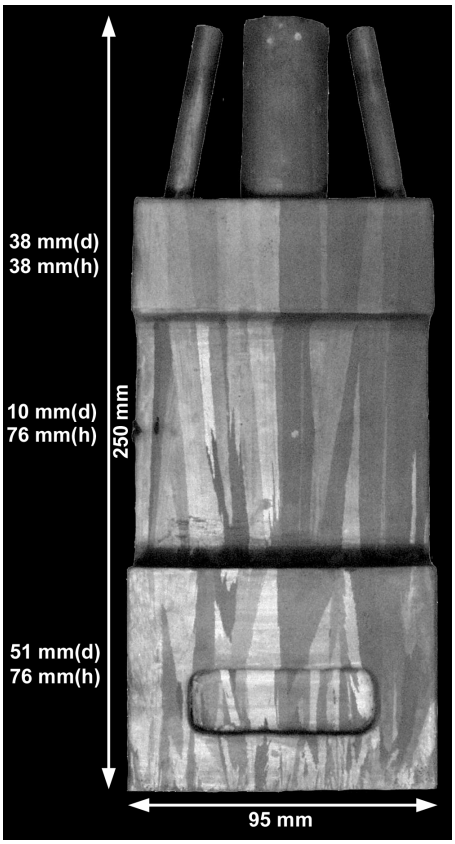

Figure 2. An example LMC casting solidified at a withdrawal rate of 2.5 mm/min in the current study shown in macro-etched condition to reveal grain structure. The height (h) and depth (d) of each casting section are noted.[16]

and with thermocouples fixed to the investment mold located approximately 10 mm away from the mold surface.

After solidification, the castings were lightly cleaned to remove mold material and macro-etched to reveal grain structure and surface casting defects. An acid bath of 80 ml HCl : 2 ml HNO_3 : 11 ml H_2O : 16 g $FeCl_3$ was used for macro etching. Samples were subsequently cut from near the center of each section of all castings. The samples were mounted and polished for examination of the surface transverse to the [001] withdrawal direction, Figure 3a. An etchant of 33 ml CH_3COOH : 33 ml H_2O : 33 ml HNO_3 : 1 ml HF was used to reveal the microstructure. PDAS (λ_1) was measured as:

$$\lambda_1 = n_P^{-½} \quad (1)$$

assuming a square array of dendrites where n_P is the number of primary dendrite cores per area.[25] After measuring PDAS, the sample surfaces were marked along a direction parallel to the secondary dendrite arms using a scribe and then sectioned along the mark. The sample was then remounted, polished, and etched for examination of the face parallel to the withdrawal direction aligned with secondary dendrite arms, Figure 3b. Secondary dendrite arm spacing (SDAS or λ_2) was measured as:

$$\lambda_2 = L / (n-1) \quad (2)$$

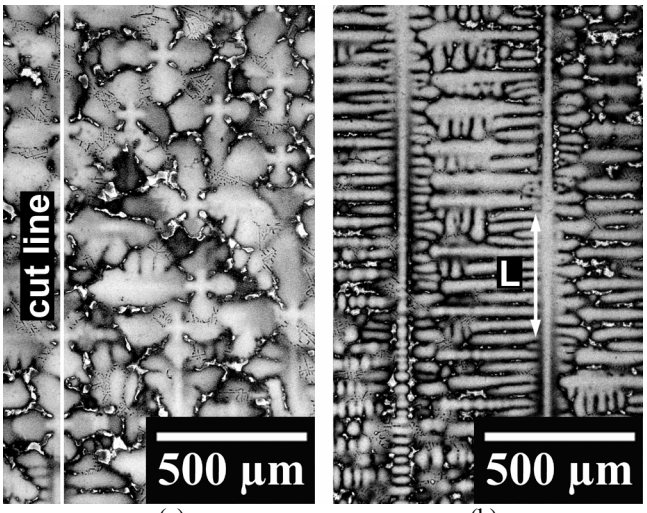

(a) (b)

Figure 3. Micrographs showing the surfaces used for measuring PDAS (a) and SDAS (b). Figure 3a shows a line indicating where samples were cut to reveal surfaces shown in figure 3b. SDAS measurements were made by drawing a line along the primary trunk and counting the number of secondary arms the line intersected.

where L is the length of a line drawn next to the primary dendrite trunk which intersects n secondary dendrite arms. At least three micrographs per sample at a magnification of 50x (a sample area of approximately 4 mm^2) were used for each measurement of PDAS and SDAS. Approximately 100 secondary dendrite arms were counted when determining the SDAS for each sample.

Results

Cooling Rates of Bridgman and LMC Castings

Experimentally determined cooling rates for Bridgman and LMC castings were plotted as a function of section thickness, Figure 4. At otherwise identical process conditions and a withdrawal rate of 2.5 mm/min, the LMC process produced cooling rates approximately double those achieved with the radiation process in

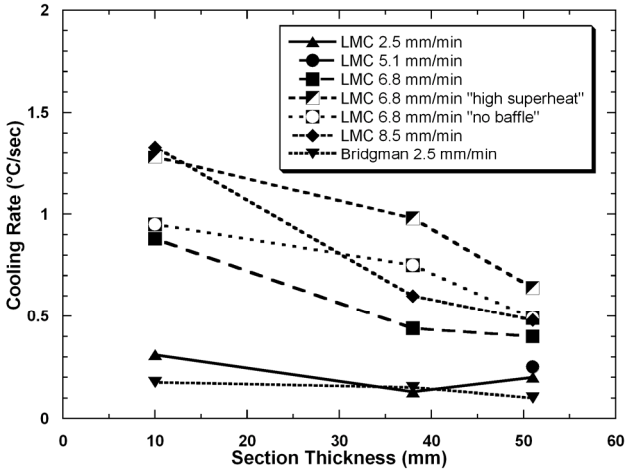

Figure 4. Experimentally measured cooling rates from various casting sections of comparable Bridgman and LMC castings. Some data absent due to thermocouple failure.

the thinnest and thickest sections. The low cooling rate in the 38 mm thick section of that LMC casting was attributed to less than ideal solidification conditions resulting from the S-L interface being located remotely from the cooling bath.[16] Faster withdrawal rates combined with liquid metal cooling resulted in significantly enhanced cooling rates compared to the Bridgman process for all casting sections.

To investigate the influence of the floating baffle and alloy superheat, three experiments were solidified with a withdrawal rate of 6.8 mm/min. The varying casting parameters produced a range of cooling rates at otherwise identical casting conditions. During the "high superheat" experiment, the increased liquid alloy temperature prior to the initiation of the withdrawal process increased the temperature difference between the hot and cool zones of the furnaces and subsequently resulted in some of the highest cooling rates recorded in these experiments. Removing the floating baffle from the coolant bath resulted in cooling rates similar to the "baseline" 6.8 mm/min casting in the thickest and thinnest sections although a notable increase in the 38 mm section was observed. Unfortunately, the increased superheat and absence of the floating baffle resulted in a downward shift of the S-L interface compared to the "baseline" casting. In both experiments, the significant downward shift of the interface below the surface of the coolant resulted in increased numbers of grain defects and changes in the dendritic structure, as discussed in more detail below.

Liquid Metal Coolant Temperatures

One of the major advantages of selecting Sn as a LMC cooling medium is the relatively low coolant operating temperature of approximately 250°C compared to 700°C for Al. Coolant temperature affects the efficiency of heat extraction during the LMC process[14] and is an important process parameter that was measured during each casting experiment. Heat was introduced into the coolant from both the mold heater, which was positioned directly above the coolant container as shown in Figure 1c, and from the mold and casting as it was immersed into the coolant. In all experiments with the floating baffle, coolant temperatures typically increased up to 50°C above the 250°C set-point shortly after withdrawal began due to lag in the coolant temperature control system and then reduced slowly towards the set-point dependent on the withdrawal rate. Slightly higher initial peak temperatures and temperatures at the end of withdrawal (Figure 5) were associated with faster withdrawal rates under conditions where the floating baffle was present. The absence of the floating baffle resulted in a significant rise in coolant temperature throughout the entire casting process. In fact, without the baffle the coolant temperature was quite high (almost 300°C) prior to withdrawal due to heating from the mold heater during the mold preheat cycle and continued to increase during withdrawal. The coolant temperature peaked at a temperature of 390°C near the end of the process.

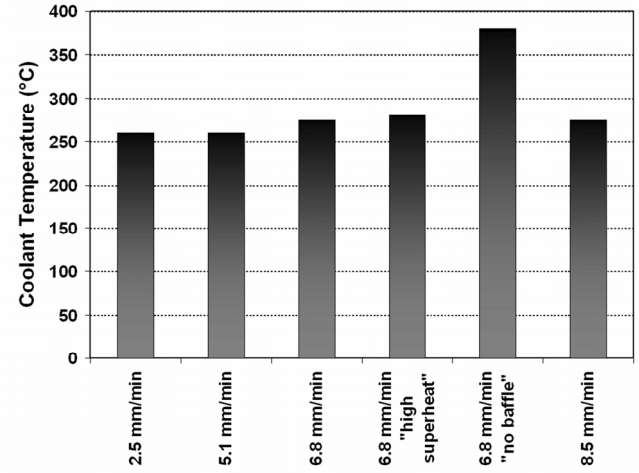

Figure 5. Liquid metal coolant (Sn) temperatures measured near the surface of the investment molds at the end of the withdrawal process.

Microstructures

The first set of experiments showed that under otherwise identical conditions and at the same withdrawal rate, the LMC process produced microstructures with a refined PDAS compared to the Bridgman process, Figure 6. The ability of the LMC process to refine PDAS was further enhanced with increased withdrawal

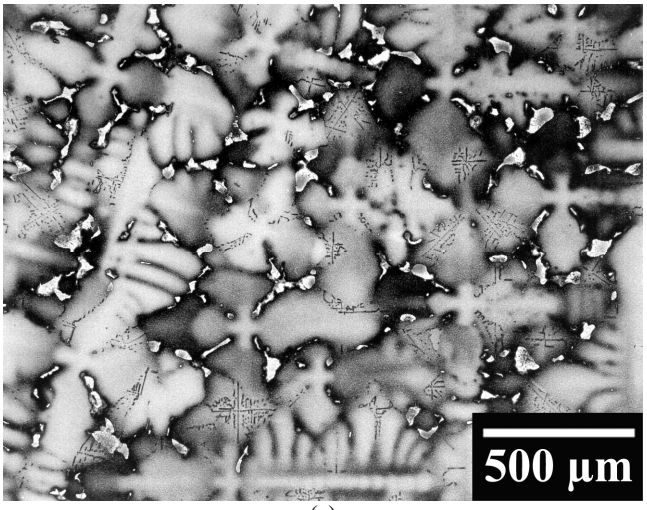

(a)

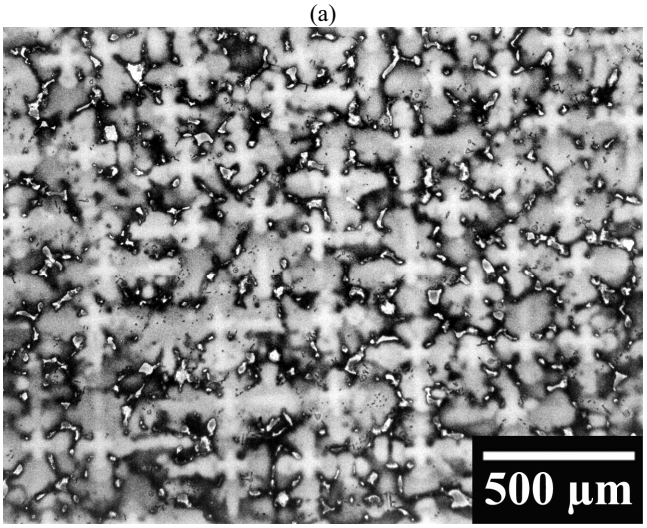

(b)

Figure 6. Sections viewed normal to the [001] growth direction showing the dendritic structure of comparable Bridgman (a) and LMC (b) castings withdrawn at 2.5 mm/min. Both sections were taken from 10 mm thick casting sections.

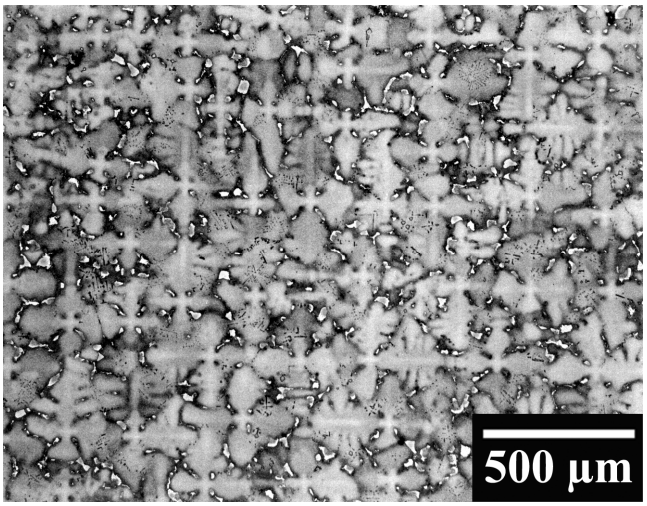

(a)

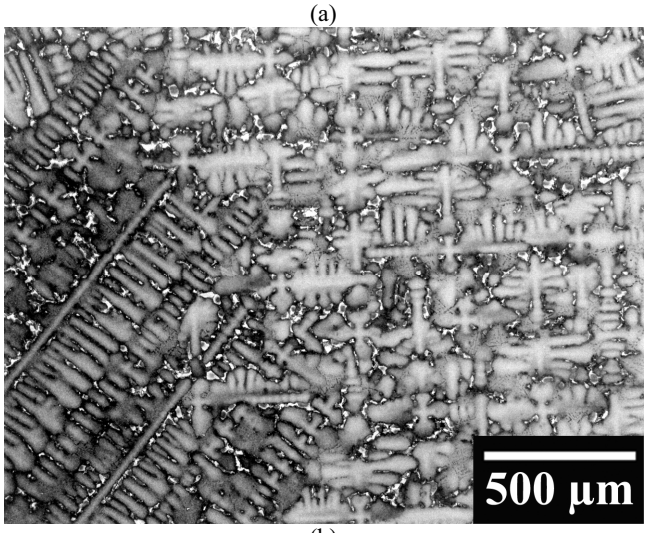

(b)

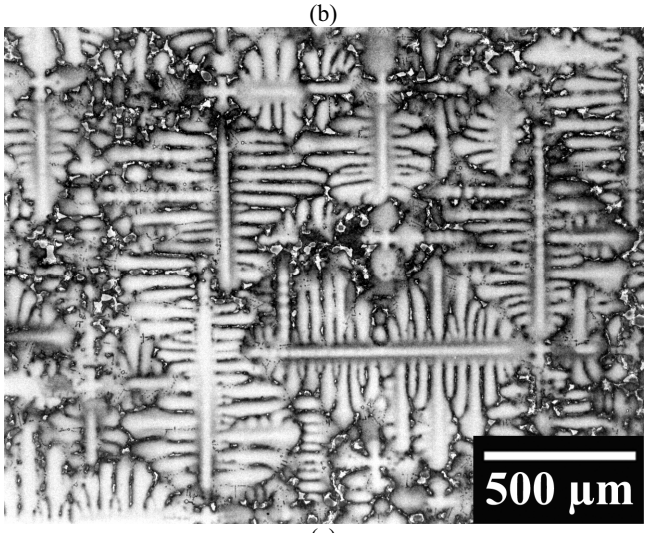

(c)

Figure 7. Sections viewed normal to the [001] growth direction from three LMC castings withdrawn at 6.8 mm/min with varying casting parameters. Sections were taken from 10 mm thick casting sections. Figures are from the "baseline" (a), "high superheat" (b), and "no baffle" (c) castings.

Table I. Casting Conditions Associated with Transverse Dendritic Growth

Casting \ Section	Bottom (51 mm thick)	Middle (10 mm thick)	Top (38 mm thick)
2.5 mm/min			
5.1 mm/min			
6.8 mm/min			
6.8 mm/min "high superheat "		X	
6.8 mm/min "no baffle "	X	X	
8.5 mm/min	X	X	

rates, Figure 7a. LMC cast microstructures also generally exhibited smaller, more uniformly distributed eutectic and carbide phases compared to the Bridgman cast microstructures.

Our prior experiments have shown the location of the solidification interface in the LMC process to be a crucial issue. At the highest withdrawal rate of 8.5 mm/min, the solid-liquid interface location shifted downward into the cooling zone of the furnace during withdrawal. If the solid-liquid interface shifted far enough below the surface of the coolant, extensive dendritic growth transverse to the withdrawal direction was observed, Figures 7b and 7c.

The casting conditions and locations within the casting that exhibited transverse dendritic growth are summarized in Table I. A minor amount of transverse dendritic growth was observed in the thinnest section of the "high superheat" 6.8 mm/min casting. Some transverse dendritic growth was also observed near the transition from the 51 mm thick section to the 10 mm thick section of the 8.5 mm/min casting due to the cross-section change. Extensive transverse dendritic growth existed throughout the entire 10 mm thick section and the upper part of the 51 mm thick section in the "no baffle" experiment withdrawn at 6.8 mm/min. As reported previously,[16] transverse dendritic growth was so severe near the top of the 10 mm thick section of the 8.5 mm/min casting that the fastest direction of dendrite growth was transverse to the withdrawal direction. The microstructure appeared to have rotated by 90° with well formed primary dendrites intersecting the (010) plane parallel to the withdrawal direction and secondary dendrites on the (001) plane transverse to the withdrawal direction. These results indicated that cross-section changes were not the primary reason for extended secondary growth. The transverse growth tended to encompass the entire cross-section of the thin casting section, but was more perceptible near the edges of the thicker section, indicating non-axial heat extraction as the primary cause, which is discussed in more detail later.

Primary Dendrite Arm Spacing. The average PDAS for each casting section was measured, Figure 8. Generally, thinner sections and faster withdrawal rates resulted in smaller PDAS for the LMC castings. The Bridgman casting had the largest PDAS. However, the "no baffle" casting had much larger PDAS measurements than the "baseline" 6.8 mm/min LMC casting in the thickest and thinnest sections. Furthermore, the PDAS measurements were almost the same as the Bridgman casting in these sections. However, comparison of Figures 6a and 7c illustrates the morphological differences in dendrite structure. The larger PDAS of the "no baffle" casting was a direct consequence of transverse dendritic growth which reduced the number of primary dendrites per area on the (001) plane. Considering the

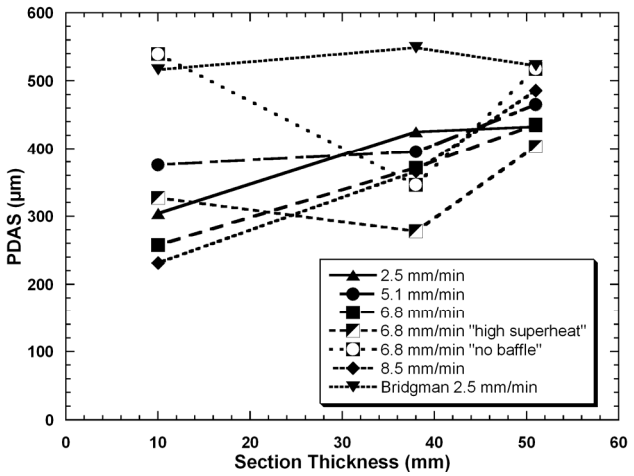

Figure 8. Average primary dendrite arm spacing measurements for each casting section plotted as a function of section thickness.

high cooling rate of the "high superheat" casting, the fact that the thinnest section only had a somewhat larger PDAS than the comparative 6.8 mm/min "baseline" casting was also likely to be associated with the transverse dendritic growth. Both the "high superheat" and "no baffle" castings had much smaller PDAS in the 38 mm thick section, reflecting the high cooling rates and the absence of transverse dendritic growth in these sections.

Secondary Dendrite Arm Spacing. Although secondary dendrite arm spacings may be influenced by local solidification time as well as coarsening, these spacings should be more useful for comparison of overall cooling conditions at the solidification front than PDAS measurements, due to a reduced influence of growth history or non-axial heat extraction.[26-28] Average SDAS measurements for each section of all castings are shown in Figure 9. The LMC casting withdrawn at 2.5 mm/min had much larger SDAS than any of the other LMC castings. Further, this was the only LMC experiment where the solid-liquid interface was located outside the coolant bath. As a result, the SDAS measurements were in the same range as the Bridgman casting. Consistent with this observation are the relatively low cooling rates measured by thermocouples inserted into the 2.5 mm/min LMC and Bridgman castings. All LMC castings withdrawn at 5.1 mm/min or faster had a similar SDAS for a given section thickness. As expected, there is a general trend toward higher SDAS at the largest section thicknesses. Interestingly, SDAS in the sections where transverse dendrite growth occurred were similar in magnitude to those where growth was primarily along the axial withdrawal direction. This indicates that SDAS measurements are likely not strongly influenced by the transverse growth phenomenon.

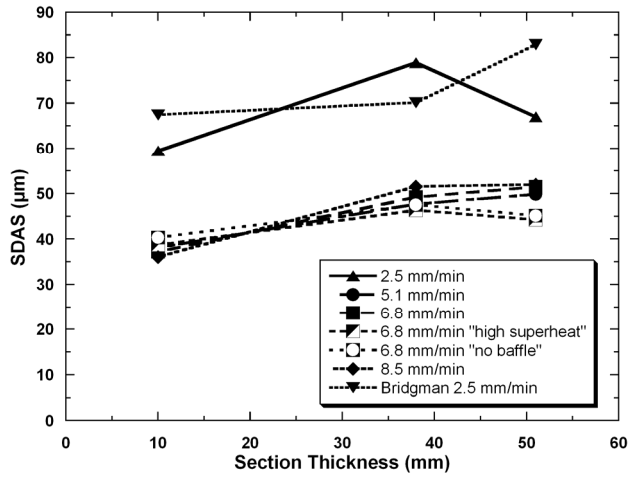

Figure 9. Average secondary dendrite arm spacing measurements for each casting section plotted as a function of section thickness.

Casting Defects

Freckle-type defects that result from thermosolutal convective instabilities driven by segregation of constituent alloying elements in the solidifying material are perhaps the most troublesome casting defects in modern DS alloys.[29] While several of these defects occurred on the Bridgman cast materials, none were observed on any of the LMC castings. Other defects unique to columnar grain castings that were characterized in this study include misoriented grains and transverse grain boundaries. All of the castings were inspected for grain boundaries transverse to the withdrawal direction, but these defects were only observed on the 8.5 mm/min casting. Misoriented grains, which were defined as a single grain being oriented more than 15° off-axis with respect to the withdrawal direction or as two grains converging or diverging at an angle greater than 20°, were by far the most common defect in all castings. It should be noted that the misoriented grains studied here are not of the type formed by the onset of thermosolutal convective instabilities that form via fragmentation processes.[9]

As illustrated in Figure 10, casting defects were significantly reduced with the LMC process for the casting configuration investigated at intermediate withdrawal rates of 5.1 and 6.8 mm/min. The 2.5 mm/min and 8.5 mm/min castings exhibited an increased number of misaligned grains due to a macroscopically curved solid-liquid interface.[7, 16, 30] Across the width of the castings in the 5.1 mm/min and all three 6.8 mm/min experiments, the grains were well aligned with the withdrawal direction, indicating a fairly flat solid-liquid interface. However, while the "baseline" casting withdrawn at 6.8 mm/min had the fewest defects and best aligned columnar grains, a change in casting

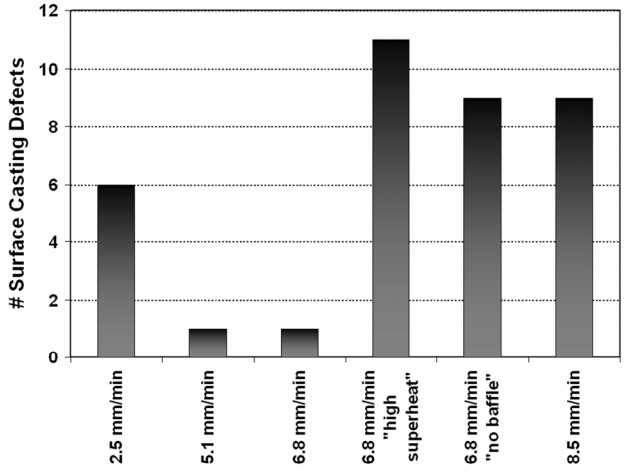

Figure 10. The number of surface casting defects (misoriented grains and transverse grain boundaries) identified for each LMC castings.

conditions resulting from increased superheat or the removal of the floating baffle resulted in degraded microstructure. Not only was the tendency for transverse dendritic growth increased, but the number of misoriented grains also increased substantially due to the shifted location of the solid-liquid interface.

Discussion

The experiments conducted in this study clearly demonstrate an enhanced cooling capacity of the LMC process compared to the Bridgman process for fairly large cross-sections. This resulted in complete elimination of defects associated with thermosolutal convective instabilities, including freckles and isolated misoriented or "spurious" grains. Higher cooling rates also resulted in a refinement of the dendritic structure and were beneficial for reducing other categories of defects as long as the growth process was not dominated by transverse dendritic growth.

Primary dendrite arm spacing has frequently been used as a measure of casting quality. It is also used to estimate cooling rates and thermal gradients through well-known relationships when direct measurement of these values are not possible.[8, 31-34] The most widely accepted models demonstrate a functional dependence of PDAS on thermal gradient (G) and solidification front velocity (V) as originally proposed by Hunt:[32]

$$\lambda_1 \propto G^{-½} * V^{-¼} \quad (3)$$

A plot of measured PDAS against experimentally determined gradient and velocity data in Figure 11 shows a moderate amount of scatter. The deviation from the relationship of equation 3, which assumes an axial gradient, was greatest in casting sections where transverse dendritic growth was prominent. These experimental points generally lie above the fit line drawn through the origin. As a result, cooling rates predicted using the relationship of equation 3 in Figure 11 and all primary dendrite arm spacing measurements would predict cooling rates higher than if transverse dendritic growth did not occur. Put another way, transverse dendritic growth inflates the PDAS of a given section predicting a smaller value of $G^{-½} * V^{-¼}$ and consequently a higher gradient at a constant withdrawal rate. The assumption of axial heat extraction clearly breaks down with transverse dendritic growth. Under these conditions, the PDAS does not provide a reliable indication of thermal gradients.

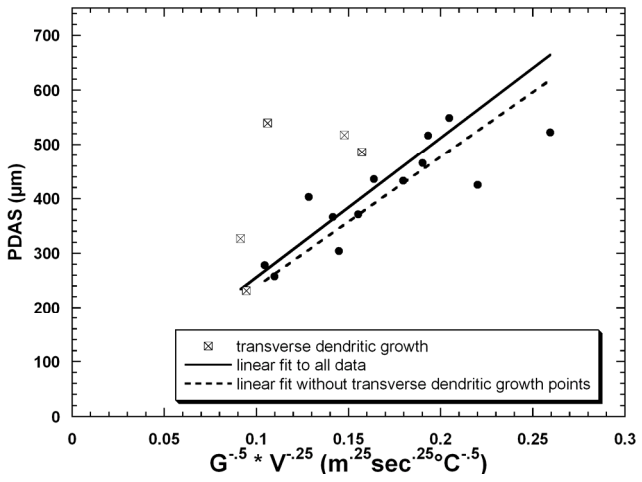

Figure 11. Primary dendrite arm spacing plotted as a function of experimentally determined $G^{-.5} * V^{-.25}$ for all LMC castings. Sections where transverse dendrite growth occurred are identified.

Generally, the SDAS can be related to local solidification time or the cooling rate (equal to the thermal gradient * solidification front velocity):[34, 35]

$$\lambda_2 \propto (G * V)^{-⅓} \quad (4)$$

Unlike PDAS, which can be influenced by dendrite growth history and interface curvature,[26-28] SDAS is primarily influenced by local solidification time and any subsequent coarsening. As illustrated by Figure 12, SDAS measurements fit this relationship with minimal scatter. Non-axial heat extraction did not result in any significant deviation across the range of conditions investigated. The lack of history effects or influence of transverse dendrite growth would seem to make SDAS a more reliable indicator of overall cooling rate.

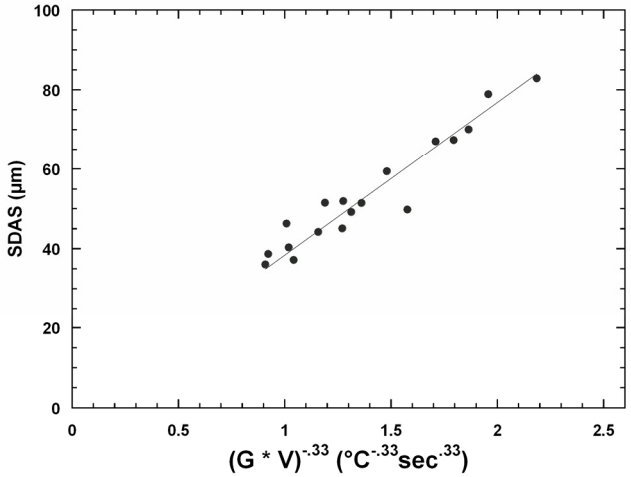

Figure 12. Secondary dendrite arm spacing plotted as a function of experimentally determined $(G * V)^{-.33}$ for all LMC castings.

The experiments conducted in this study demonstrate that cooling rate alone is not a good predictor of defect formation. Within the high cooling rate range for the 6.8 mm/min castings, there was a wide variation in tendency for grain defect formation. Comparing the lack of defects in the "baseline" 6.8 mm/min casting and the high defect occurrence of the "high superheat" and "no baffle" experiments shown in Figure 10 and the corresponding microstructures in Figures 7a, b and c, it is apparent that transverse dendrite growth is associated with defect occurrence for the high cooling rate castings. The number of misoriented grains increased with the degree of transverse dendritic growth, which, in turn, was influenced by solidification front shape and location in the cooling bath. Aspects of the LMC process that lead to transverse dendrite growth must be better understood to fully optimize this process. Further, it is not clear how much effect transverse growth will have on mechanical properties of these materials. In the extreme case where the direction of fastest growth is transverse to the withdrawal direction the possibility of transverse grain boundaries or defects in the center of the castings

is increased since the growth is presumably from the surface inward.

The morphological differences due to transverse dendritic growth are shown in Figures 6 and 7. The large differences in morphologies are apparently the result of off-axis heat flow and non-planar interface shape. The origins of non-axial heat flow in the LMC process are related to the location of the S-L interface relative to the cooling bath. The ideal location of the S-L interface during LMC is near or just below the surface of the cooling bath.[16, 36] At high withdrawal rates, the cooling capacity of the tin bath was not able to balance the heat input and a downward shift of the S-L interface occurred. As the solidification front moved into the cooling zone at these high withdrawal rates, the sides of the mold surrounding unsolidified metal were exposed to strong transverse component of cooling from the coolant bath. This situation resulted in a S-L interface curved away from the liquid metal. Further, transverse dendritic growth was most pronounced near the edges of the casting sections, consistent with the presumed heat flow, which was likely to be more axial near the center of the casting.

The floating baffle was clearly effective in controlling solid-liquid interface location and shape. In the "no baffle" experiment withdrawn at 6.8 mm/min, the solid-liquid interface shifted downward significantly. The "no baffle" casting exhibited transverse dendritic growth and an increased number of misoriented grains compared to the "baseline" casting withdrawn at 6.8 mm/min.

Investigations aimed at producing large castings with the LMC process using tin and aluminum as cooling media show promising results.[4, 6, 15-16, 21] It is clear that LMC casting parameters must be optimized in order to fully exploit the benefits of the process. Specifically, control of the S-L interface is imperative to optimizing the process. The position of the S-L interface depends on many factors including casting dimensions, coolant temperature, baffle thickness and nature, superheat temperature, and mold properties. These experiments have highlighted an important, but indirect benefit of the LMC-Sn process: the floating alumina baffle. The baffle results in a more planar solidification front and most importantly helps to insulate the coolant from the furnace heater. There are a number of baffle variables that could be optimized to further enhance the process. The baffle material and its thermal insulating properties are most important. The size of the baffle beads, packing density, and overall thickness of the baffle certainly will influence the solidification conditions and could be tailored for better control of the S-L interface. Ultimately thermal modeling is necessary to optimize and fully understand the LMC process harnessing its full potential.

Conclusions

1. Directional solidification with a liquid tin cooling medium provides the capability for higher cooling rates and smaller PDAS and SDAS in large cross-section castings compared to the Bridgman process.
2. Solid-liquid interface location relative to the cooling bath affects the solid-liquid interface shape, macroscopic grain structure, degree of transverse heat extraction, and the propensity to form casting defects in the LMC process.
3. There is a tendency for transverse dendrite growth at high withdrawal rates under conditions where the solidification front shifts significantly below the surface of the coolant bath.
4. Withdrawal rate and superheat in the solidifying casting influence the solid-liquid interface location and, consequently, the degree of radial heat extraction during solidification.
5. The floating baffle is an essential element of the LMC process that is quite effective as a thermal barrier between the hot and cool zones of the furnace and for controlling the solid-liquid interface location and axial heat extraction during liquid metal cooling.

Acknowledgements

The authors would like to acknowledge the assistance of and useful discussions with: Q. Feng, C.J. Torbet, and B. Tryon of the University of Michigan; S. Tin of the University of Cambridge; S. Balsone and J. Schaeffer of General Electric Power Systems. The support provided by T. Van Vranken and L. Graham of PCC Airfoils, Inc. is greatly appreciated. The funding provided by General Electric Power Systems, General Electric Global Research, and the National Science Foundation grant number DMR-0127689 are also gratefully acknowledged.

References

1. M. Gell, C.P. Sullivan, and F.L. VerSnyder, "Casting and Properties of Unidirectionally Solidified Superalloys," *Solidification Technology*, ed. J.J. Burke, M.C. Flemings, and A.E. Gorum (Chestnut Hill, MA: Brook Hill, 1974), 141-164.

2. R.W. Smashey, "Apparatus and Method for Directional Solidification" (U.S. Patent No. 3,897,815), 1975.

3. C.H. Lund and J. Hockin, "Investment Casting," *The Superalloys*, ed. C.T. Sims and W.C. Hagel (New York: John Wiley & Sons, 1972), 403-425.

4. A. Kermanpur, M. Rappaz, N. Varahram, and P. Davami, "Thermal and Grain-Structure Simulation in a Land-Based Turbine Blade Directionally Solidified with the Liquid Metal Cooling Process," *Metall. Trans. B*, 31B (6) (2000), 1293-1304.

5. M. Konter, E. Kats, and N. Hofmann, "A Novel Casting Process for Single Crystal Gas Turbine Components," *Superalloys 2000*, ed. T.M. Pollock, R.D. Kissinger, R.R. Bowman, K.A. Green, M. McLean, S.L. Olson, and J.J. Schirra (Warrendale, PA: TMS, 2000), 189-200.

6. F. Hugo, U. Betz, J. Ren, S.-C. Huang, J.A. Bondarenko, and V. Gerasimov, "Casting of Directionally Solidified and Single Crystal Components Using Liquid Metal Cooling (LMC)," *International Symposium on Liquid Metal Processing and Casting*, ed. A. Mitchell, L. Ridgway, and M. Baldwin (New York, NY: AVS, 1999), 16-30.

7. N. D'Souza, M.G. Ardakani, M. McLean, and B.A. Shollock, "Directional and Single-Crystal Solidification of Ni-Base Superalloys: Part I. The Role of Curved Isotherms on Grain Selection," *Metall. Trans. A*, 31A (11) (2000), 2877-2886.

8. G.K. Bouse and J.R. Mihalisin, "Metallurgy of Investment Cast Superalloy Components," *Superalloys, Supercomposites and Superceramics*, ed. J.K. Tien and T. Claufield (San Diego, CA: Academic Press, 1989), 99-148.

9. T.M. Pollock and W.H. Murphy, "The Breakdown of Single-Crystal Solidification in High Refractory Nickel-Base Alloys," *Metall. Trans. A*, 27A (4) (1996), 1081-1094.

10. P.N. Quested and M. McLean, "Effect of Variations in Temperature Gradient and Solidification Rate on Microstructure and Creep Behaviour of IN 738LC," *Solidification Technology in the Foundry and Cast House* (London: The Metals Society, 1983), 586-591.

11. P.N. Quested, P.J. Henderson, K. Menzies, and M. McLean, "Mechanical Behaviour of Ni-Cr-Base Superalloys in Forms and Conditions Representative of Service" (NPL Report DMA(A)94, COST 50, December, 1984).

12. P.N. Quested and S. Osgerby, "Mechanical Properties of Conventionally Cast, Directionally Solidified and Single-Crystal Superalloys," *Mat. Sci. Technol.*, 2 (5) (1986), 461-475.

13. J. Grossman, J. Preuhs, W. Esser, and R.F. Singer, "Investment Casting of High Performance Turbine Blades by Liquid Metal Cooling - A Step Forward Towards Industrial Scale Manufacturing," *International Symposium on Liquid Metal Processing and Casting*, ed. A. Mitchell, L. Ridgway, and M. Baldwin (New York, NY: AVS, 1999), 31-40.

14. A. Lohmüller, W. Esser, J. Gossmann, M. Hördler, J. Preuhs, and R.F. Singer, "Improved Quality and Economics of Investment Castings by Liquid Metal Cooling--The Selection of Cooling Media," *Superalloys 2000*, ed. T.M. Pollock, R.D. Kissinger, R.R. Bowman, K.A. Green, M. McLean, S.L. Olson, and J.J. Schirra (Warrendale, PA: TMS, 2000), 181-188.

15. A.J. Elliott, T.M. Pollock, S. Tin, W.T. King, S.-C. Huang, and M.F.X. Gigliotti, "Defect Reduction in Large Superalloy Castings by Liquid-Tin Assisted Solidification," *Parsons 2003: Engineering Issues in Turbine Machinery, Power Plant and Renewables*, ed. A. Strang, R.D. Conroy, W.M. Banks, M. Blackler, J. Leggett, G.G. McColvin, S. Simpson, M. Smith, F. Starr, and R.W. Vanstone (London: Maney, 2003), 649-661.

16. A.J. Elliott, S. Tin, W.T. King, S.-C. Huang, M.F.X. Gigliotti, and T.M. Pollock, "Directional Solidification of Large Superalloy Castings with Radiation and Liquid Metal Cooling (LMC): A Comparative Assessment," *Metall. Trans. A*, (in press) (2004).

17. F.D. Lemkey, "Casting and Properties of Directionally Solidified Eutecic Superalloys," *Solidification Technology*, ed. J.J. Burke, M.C. Flemings, and A.E. Gorum (Chestnut Hill, MA: Brook Hill, 1974), 165-186.

18. A.F. Giamei and J.G. Tschinkel, "Liquid Metal Cooling: A New Solidification Technique," *Metall. Trans. A*, 7A (9) (1976), 1427-1434.

19. V.V. Gerasimov, "Method of Casting Parts with Directed and Mono-Crystal Structure" (U.S.S.R. Patent No. 2836278/22-02), 1981.

20. G.B. Stroganov, A.V. Logunov, V.V. Gerasimov, and E.L. Kats, "High-Rate Directed Crystallization of Heat Resistant Alloys," *Casting Production (in Russian)*, 12 (1983), 20-22.

21. T.J. Fitzgerald and R.F. Singer, "An Analytical Model for Optimal Directional Solidification Using Liquid Metal Cooling," *Metall. Trans. A*, 28A (6) (1997), 1377-1383.

22. T.J. Fitzgerald, R.F. Singer, and P. Krug, "Method and Device for Directionally Solidifying a Melt" (European Patent No. EP0775030), 1997.

23. E.W. Ross, C.S. Wukusick, and W.T. King, "Nickel-Based Superalloys for Producing Single Crystal Articles Having Improved Tolerance to Low Angle Grain Boundaries" (U.S. Patent No. 5,399,313), 1995.

24. E.W. Ross and K.S. O'Hara, "Rene N4: A First Generation Single Crystal Turbine Airfoil Alloy with Improved Oxidation Resistance, Low Angle Boundary Strength and Superior Long Time Rupture Strength," *Superalloys 1996*, ed. R.D. Kissinger, D.J. Deye, D.L. Anton, A.D. Cetel, M.V. Nathal, T.M. Pollock, and D.A. Woodford (Warrendale, PA: TMS, 1996), 19-25.

25. D.G. McCartney and J.D. Hunt, "Measurement of Cell and Primary Dendrite Arm Spacings in Directionally Solidified Aluminum Alloys," *Acta Metall.*, 29 (11) (1981), 1851-1863.

26. H. Weidong, G. Xingguo, and Z. Yaohe, "Primary Spacing Selection of Constrained Dendritic Growth," *J. Cryst. Growth*, 134 (1993), 105-115.

27. X. Wan, Q. Han, and J.D. Hunt, "Different Growth Regimes During Directional Dendritic Growth," *Acta Mater.*, 45 (10) (1997), 3975-3979.

28. W. Wang, P.D. Lee, and M. McLean, "Simulation of the History Dependence of Primary Dendrite Spacing in Directional Solidification," *Modelling of Casting, Welding and Advanced Solidification Processes X*, ed. D.M. Stefanescu, J. Warren, J. Jolly, and M. Krane (Warrendale, PA: TMS, 2003), 83-90.

29. S.M. Copley, A.F. Giamei, S.M. Johnson, and M.F. Hornbecker, "Origin of Freckles in Unidirectionally Solidified Castings," *Metall. Trans.*, 1 (8) (1970), 2193-2204.

30. R.M. Ward, S.M. Johnson, and M.H. Jacobs, "Liquid Pool Shapes During the Plasma Remelting of a Nickel-Based Superalloy," *International Symposium on Liquid Metal Processing and Casting*, ed. A. Mitchell and P. Auburtin (New York, NY: AVS, 1997), 978-109.

31. M.C. Flemings, *Solidification Processing* (New York, NY: McGraw-Hill, 1974).

32. J.D. Hunt, "Cellular and Primary Dendrite Arm Spacings," *Solidification and Casting of Metals*, ed. J.D. Hunt (London: The Metals Society, 1979), 3-9.

33. M. McLean, *Directionally Solidified Materials for High Temperature Service* (London: The Metals Society, 1983).

34. W. Kurz and D.J. Fisher, *Fundamentals of Solidification*, 4th rev. ed. (Enfield, NH: Trans Tech Publications, 1998).

35. H. Biloni and W.J. Boettinger, "Solidification," *Physical Metallurgy*, ed. R.W. Cahn and P. Haasen, Vol. 1 (New York, NY: North-Holland, 1996), 669-842.

36. P.N. Quested and M. McLean, "Solidification Morphologies in Directionally Solidified Superalloys," *Mater. Sci. Eng.*, 65 (1) (1984), 171-180.